

# Long Endurance and Long Distance Trajectory Optimization for Engineless UAV by Dynamic Soaring

B. J. Zhu<sup>1,2</sup>, Z. X. Hou<sup>1</sup>, X. Z. Wang<sup>3</sup> and Q. Y. Chen<sup>1</sup>

**Abstract:** The paper presents a comprehensive study on the performance of long endurance and long distance trajectory optimization of engineless UAV in dynamic soaring. A dynamic model of engineless UAV in gradient wind field is developed. Long endurance and long distance trajectory optimization problems are modelled by non-linear optimal control equations. Two different boundary conditions are considered and results are compared: (i) open long endurance pattern, (ii) closed long endurance pattern, (iii) open long distance pattern. In patterns of (i) and (ii), the UAV return to original position with the maximum flying time in pattern (ii), and in patterns of (ii) and (iii), the maximum distance and minimum flying time occur in pattern (iii). The energy variations trends of three patterns have shown a fairly similar pattern. In the gradient wind field, long endurance and long distance are two independent flight patterns for engineless UAV by dynamic soaring.

**Keywords:** long endurance, long distance, dynamic soaring, non-linear optimal control.

## 1 Introduction

Long endurance and long distance are key operational factors of unmanned aerial vehicle utility. Be limited by the fuel capacity of unmanned aerial vehicle (UAV), people propose to use engineless flight. In many flight environments of UAV, there are existed energy available in the atmosphere that can be used to increase endurance and distance, such as wind gradients. To extract energy from the wind gradients is generally referred to as dynamic soaring [Bower (2011)].

---

<sup>1</sup> College of Aerospace Sciences and Engineering, National University of Defense Technology, Changsha, 410073, China.

<sup>2</sup> Corresponding author. Tel: +8613548776007; Fax: +86-0731-84573189;  
E-mail: jackerzhu@163.com

<sup>3</sup> Chongqing Key Laboratory of Heterogeneous Material Mechanics, Department of Engineering Mechanics, Postdoctoral Station of Mechanics, Chongqing University, Chongqing 400040, China.

As a matter of fact, there are many large-sized birds in the nature that they make use of gradient wind to enhance their flight ability, such as albatrosses [Denny (2009); Traugott et al. (2010)]. By means of dynamic soaring, the wandering albatrosses achieve flights of several thousands of miles without flapping their wings [Richardson (2011)]. Lord Rayleigh (1883) published “The soaring of birds” on the Nature in 1883, which is regarded as the first research paper about dynamic soaring. The wandering albatross’ parameters were studied by Sachs (2005), with its 3.4-m wing span is of similar size to a small UAV. That is to say, the albatross’ flight performance can be taken as a baseline model against which dynamic soaring performance of a small UAV. And due to friction between the moving air mass and the surface, wind gradients are commonly found near the surface, especially in the interactions between the ocean and lower atmosphere. So there are many missions that the dynamic soaring UAV would be well suited to perform.

For the principle of dynamic soaring, Clarence (1964) established many mathematical models to analyse the dynamic soaring flight of albatross. Lawrance and Sukkarieh (2011) presented a path planning and dynamic target assignment algorithm to generate energy-gain paths from the current wind estimate. Optimization technique was applied for determining dynamic soaring trajectories which yield the maximum energy transfer from the moving air to the aircraft [Sachs and Orlando (2003)]. Akhtar et al. (2009) described a trajectory generation technique suitable for real-time implementation, which would allow on-line computation of the next loop during the current trajectory loop. In order to estimate wind field for autonomous dynamic soaring, Lawrance et al. (2011) provided a method for taking direct observations of the wind during flight and creating a wind to direct future exploration. With regards to the wind condition for dynamic soaring, Sachs et al. (1989) gave a analytical solution of minimal wind condition trajectories for dynamic soaring, Deitter et al. (2009) generated optimal trajectories for minimal and maximal wind conditions. The sufficient conditions for dynamic soaring were computed by Bencatel et al. (2014) through a heuristic method that optimized the flight trajectories. Effects of wind gradient slope and wind profile non-linearity on dynamic soaring patterns were examined by Zhao (2004).

From these research findings, it can be found that the UAV could extract enough energy from wind gradients for its flight by means of dynamic soaring. Meanwhile, these achievements are very useful in studying the relationship between energy variation and optimal trajectory in dynamic soaring. This paper extends these works by considering long endurance and long distance in dynamic soaring.

Since wind gradients can be regarded as an energy resource, we can do some mission planning base on dynamic soaring. Whether war or peace, an aircraft is often wished to best advantage for some particular purpose. It may be to fly as long en-

duration as possible, or to achieve the maximum distance on a given quantity of fuel. In fact, long endurance and long distance are two goals contradicted each other. If an aircraft wants to stay in the air for the longest possible time, which is not the same consideration as flying for maximum range [Kermode (2006)], to get maximum endurance, it must use the least possible fuel in a given time, that is to say, it must use minimum power. Power means drag times velocity, the velocity is the air speed of aircraft. If it wants to move an aircraft with a distance of the maximum number of metres, it must pull the aircraft with the minimum thrust. Least thrust means least drag, flying for maximum distance means minimum drag, which is the essence of flying for distance. In the same way, in a dynamic soaring system, long-endurance dynamic soaring and long-distance dynamic soaring are two modes of energy extraction in this time scale separation, which can be used to treat each mode almost independently.

There are many optimization methods used for investigating trajectories for dynamic soaring in specific conditions [Sachs and Orlando (2003); Zhao (2004); Zhao and Qi (2004); Sachs (2005); Guo and Zhao (2010); Vincent et al. (2013)]. Inspired by the optimization methods by Reference [Zhao (2004)], long endurance and long distance are considered as optimal goals in energy-gaining trajectories of dynamic soaring, and obtained the optimal trajectories in which the UAV passes through wind gradients with specific conditions on its relative orientation (heading, climb rate and bank angle), aerodynamic load factor, and airspeed.

The remainder of the paper is organized as follows. Modeling and analysis are introduced in Section 2. Simulation results and associated discussion are given in Section 3. Finally, the concluding remarks are made in Section 4.

## 2 Modeling and analysis

### 2.1 The gradient wind model

The aircraft can extract energy from the wind field when it is following a favorable dynamic soaring trajectory. So in the process of optimization, there is a mathematical model of the gradient wind profile needed. Due to the friction between the wind and the surface, it is assumed that the aircraft flies over a flat surface. To make the calculation, only the horizontal wind component is simply considered, the wind component of other direction is zero. In the wind field, the horizontal wind speed increases with the increasing of altitude, and air density is assumed to be constant [(Zhao and Qi (2004)]. The relation between wind speed  $W_x$  and height above the surface  $z_i$  is given by

$$W_x = \beta z_i \quad (1)$$

where  $W_x$  is the wind speed at height  $z$ , the value of  $\beta$  is defined by the wind conditions. In this paper, the wind velocity is nearly zero at the surface.

### 2.2 Motion equations of dynamic soaring

In dynamic soaring, the rotational dynamics are assumed to be far faster than the translational dynamics, the rotations is not considered in the flight model. In this section the dynamic equation for a soaring aircraft in three degrees of freedom (3DOF) is discussed. There is no propulsion system on the aircraft. For a point mass model, the forces and angles used in this model are shown in Fig. 1. The inertial wind speed components in the  $x$ ,  $y$ , and  $z$  directions are respectively denoted as  $W_x$ ,  $W_y$  and  $W_z$ . Note that  $W_y = W_z=0$ ,  $W_x$  is the function of wind.

In Fig.1, there are three applied forces accounted for in this model: lift ( $L$ ), drag ( $D$ ) and gravitational force ( $mg$ ),  $\gamma$  is flight path angle,  $\psi$  is heading angle,  $\phi$  is bank angle,  $V$  represents the air speed.

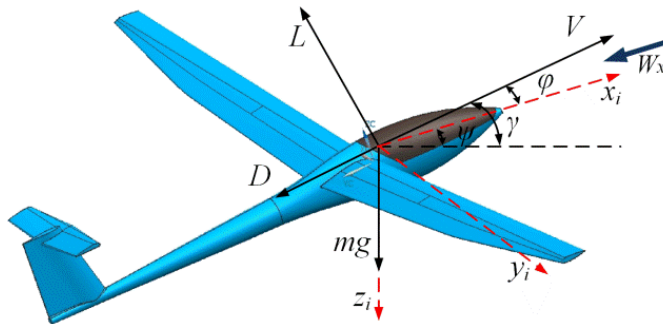


Figure 1: Air-relative velocity and applied forces for the UAV.

Using the standard formulations for lift and drag force:

$$L = \frac{1}{2} \rho S C_L V^2 \tag{2}$$

$$D = \frac{1}{2} \rho S C_D V^2 \tag{3}$$

$$C_D = C_{D0} + K C_L^2 \tag{4}$$

where  $\rho$  is air density ( $\text{kg/m}^3$ ),  $S$  is wing area ( $\text{m}^2$ ),  $C_L$  is lift coefficient,  $C_D$  is drag coefficient,  $V$  is the airspeed of the aircraft,  $C_{D0}$  is the parasitic drag coefficient and  $K$  is the induced drag coefficient. Note that

$$K = \left( 4 \left( \frac{L}{D} \right)_{\max}^2 C_{D0} \right)^{-1} \tag{5}$$

where  $(L/D)_{max}$  is the maximum lift over drag ratio, which, together with  $C_{D0}$ , is the most important aircraft aerodynamic efficiency parameter and fully defines the aerodynamic drag polar.

Applying Newton's Second Law to analyze the forces acted on the aircraft, the results are shown in Eqs. (6):

$$\begin{cases} m\ddot{x}_i = -D \cos \gamma \cos \psi + L(-\sin \gamma \cos \psi \cos \phi - \sin \psi \sin \phi) \\ m\ddot{y}_i = -D \cos \gamma \sin \psi + L(-\sin \gamma \sin \psi \cos \phi + \cos \psi \sin \phi) \\ m\ddot{z}_i = D \sin \gamma + L(-\cos \gamma \cos \phi) + mg \end{cases} \quad (6)$$

The kinematic equations is given by Eqs. (7):

$$\begin{cases} \dot{x}_i = V \cos \gamma \cos \psi - W_x \\ \dot{y}_i = V \cos \gamma \sin \psi \\ \dot{z}_i = -V \sin \gamma \end{cases} \quad (7)$$

The kinematic equations (Eqs. (7)) is differentiated with respect to time, and the following equations can be obtained.

$$\begin{cases} \ddot{x}_i = \dot{V} \cos \gamma \cos \psi - \dot{\gamma} V \sin \gamma \cos \psi - \dot{\psi} V \cos \gamma \sin \psi - \dot{W}_x \\ \ddot{y}_i = \dot{V} \sin \psi \cos \gamma + \dot{\psi} V \cos \psi \cos \gamma - \dot{\gamma} V \sin \psi \sin \gamma \\ \ddot{z}_i = -\dot{V} \sin \gamma - \dot{\gamma} V \cos \gamma \end{cases} \quad (8)$$

Combining Eqs. (6) and Eqs. (8), then there is:

$$\begin{cases} m\dot{V} = -D - mg \sin \gamma - m\dot{W}_x \cos \gamma \cos \psi \\ mV \cos \gamma \dot{\psi} = L \sin \phi - m\dot{W}_x \sin \psi \\ mV \dot{\gamma} = L \cos \phi - mg \cos \gamma + m\dot{W}_x \sin \gamma \cos \psi \end{cases} \quad (9)$$

In these sets of kinematic equations (Eqs. (6) and Eqs. (8)), the state variables are  $[x_i, y_i, z_i, V, \psi, \gamma]$ , and the control variables are  $[C_L, \phi]$ . The lift coefficient is primarily a function of the angle of attack, the angle of attack can be effected through the elevator motion, so the lift coefficient is used as a control variable. Eqs. (9) is the equations of motion in the wind relative reference frame. The wind relative reference frame is a noninertial frame of reference. There has a fictitious force ( $F$ ) applied to it [José and Saletan (1998); Deittert, Richards et al. (2009)],

$$F = -m \frac{dW_x}{dt} = -m \frac{dW_x}{dz} \cdot \frac{dz}{dt} = m\beta V \sin \gamma \quad (10)$$

The fictitious force ( $F$ ) is created by wind, so the direction of the force is the same as the wind, also in the  $X$  direction. Of course, the fictitious force can be used to do

work [José and Saletan (1998)]. The power of the inertial force can be expressed as,

$$P = F\dot{x}_i = m\beta V^2 \sin \gamma \cos \gamma \cos \psi \quad (11)$$

Because of the inertial force, the UAV can extract energy from the wind gradient. Eq. (11) shows that to extract energy from the wind field depends on the product of  $\sin(\gamma)$  and  $\cos(\psi)$ . In a cycle of dynamic soaring, the energy ( $E$ ) extracted from the wind gradient can be illustrated as

$$E = \int_0^T m\beta V^2 \sin \gamma \cos \gamma \cos \psi dt \quad (12)$$

where,  $T$  is the cycle of dynamic soaring.

Because the ability of UAV to continue flying as the aerodynamic forces generated on UAV depend on the airspeed, the air relative kinetic energy for UAV is more reliable. The air relative total energy of UAV can be represented as,

$$E_{air} = -mgz_i + \frac{1}{2}mV^2 \quad (13)$$

Eq. (13) is differentiated with respect to time resulting in Eq. (14):

$$\dot{E}_{air} = -mg\dot{z}_i + mV\dot{V} \quad (14)$$

Combined with Eqs. (9), (14), gives,

$$\dot{E}_{air} = -DV + m\beta V^2 \sin \gamma \cos \gamma \cos \psi \quad (15)$$

From comparison between Eq. (11) and Eq. (15), it can be found that the power of the inertial force created by wind gradient is the only source of energy which the UAV extracted from the flight environment. That is to say, in order to extract energy from the wind, the UAV must fly in regions of gradient wind field ( $\beta \neq 0$ ). Meanwhile, from Eq. (15), it is obviously energy is always lost due to drag.

### 2.3 The boundary constraint of trajectory

Dynamic soaring requires the vehicle to be manoeuvred in a coordinated fashion through the wind gradient. Energy-gaining trajectories are ones in which the vehicle passes through gradients with specific conditions. First of all, setting the initial conditions of optimization calculation. Subject to Eqs. (16), the following initial conditions:

$$\begin{cases} x(t_0) = 0 \\ y(t_0) = 0 \\ z(t_0) = 0 \\ \gamma(t_0) = 0 \end{cases} \quad (16)$$

where  $t_0$  means the initial time.

Of course, the trajectory of optimization should respect the aircraft's operational and performance limitations. The following path constraints:

$$z_i \geq 0 \tag{17}$$

$$C_{Lmin} \leq C_L \leq C_{Lmax} \tag{18}$$

$$-\phi_{min} \leq \phi \leq \phi_{max} \tag{19}$$

$$n \leq n_{max} \tag{20}$$

The aircraft are flying above the ground,  $z_i$  never becomes negative. The lift coefficient  $C_L$  keeps in positive due to the attack angle in dynamic soaring never becoming negative. Of course, there are a range of trajectories produced energy gains. Optimum trajectories with energy gains can sustain total energy, there may be selected as those that maximise the distance of endurance. And the set of terminal constraints are selected to enforce a basic periodic dynamic soaring flight.

$$V(t_f) = V(t_0) \tag{21}$$

$$z_i(t_f) = z_i(t_0) \tag{22}$$

$$\gamma(t_f) = \gamma(t_0) \tag{23}$$

$$\psi(t_f) = \psi(t_0) \tag{24}$$

where  $t_f$  is the terminal time. Eq. (21) and Eq. (22) lead to energy-neutral dynamic soaring. Dynamic soaring path constraints are generally needed due to bound on the load factor and seeability. The load factor ( $n$ ) is defined as:

$$n = \frac{L}{mg} \leq n_{max} \tag{25}$$

The constraint on the load factor ( $n$ ) affects the maximum airspeed. On the other hand, the maximum value of the load factor ( $n_{max}$ ) can't exceed a certain value. In this paper, according to the characteristics of the aircraft, the following values of flight constraints are used [Zhao and Qi (2004)]:

$$C_{Lmin} = 0, \quad C_{Lmax} = 1.5, \quad \phi_{max} = 80^\circ, \quad n_{max} = 5 \tag{26}$$

## 2.4 The energy calculation formulaes for distance and endurance in dynamic soaring

We can determine the aerodynamic configuration which provides the minimum energy expenditure:

$$D = n \cdot mg \cdot \frac{D}{L} = n \cdot mg \cdot \frac{C_D}{C_L} \quad (27)$$

In this paper, the energy required for the flight is absorbed from the flight environment, it is difficult to find out the relationships between energy absorb and flight types. But it is plain and simple to calculate the energy loss in dynamic soaring. The energy loss equations for distance and endurance in dynamic soaring are different with each other. Through the following calculation, it could be found that the control variables are play different roles in these two processes. According to the constraints and optimization goals, there are three patterns.

Pattern (i): in this pattern, in order to maximize the endurance, it need to maximize the amount of time that the aircraft stays in the air. For endurance, the consumed energy (W) is:

$$W = Dv \cdot t \quad (28)$$

The above equation (Eq. (28)) can be changed into:

$$W = \frac{1}{2} \rho S C_D v^3 t = \frac{\sqrt{2}(mg)^{3/2}}{\sqrt{\rho S}} \frac{C_D}{(C_L/n)^{3/2}} t \quad (29)$$

If the consumed energy (W) equals to the extracted energy (E), combined with Eqs. (12) and (29),

$$t = \frac{\int_0^T \beta V^2 \sin \gamma \cos \gamma \cos \psi dt}{\frac{\sqrt{2}mg^{3/2}}{\sqrt{\rho S}} \frac{C_D}{(C_L/n)^{3/2}}} \quad (30)$$

The endurance is also a multi parameters optimization problem. In this problem formulation, the maximum cycle time of a dynamic soaring cycle is meaningful to determine the endurance of UAV flight. Mathematically,

$$\max J = t_f \quad (31)$$

subject to Eqs. (9).  $t_f$  is the maximum flight time. The constraint conditions are listed in Part 2.3. The vehicle returns to its original kinematic velocity state and height, but not the original position.

Pattern (ii): in order to make the results of long endurance more convincing, there are two possibilities need to be considered. One is the UAV returns to its original kinematic velocity state and height, but not the original position, such as pattern (i), the other is the UAV returns to its original kinematic velocity state and the original position. So in the process of long endurance trajectory optimization when the UAV returns to original position, it needs some other constraint conditions to get the satisfactory results.

$$x(t_f) = x(t_0) \tag{32}$$

$$y(t_f) = y(t_0) \tag{33}$$

Pattern (iii): in order to maximize the distance, it should reduce the drag as much as possible in the process of flight. For distance, the consumed energy (W) is:

$$W = D \cdot d = mg \cdot \left( \frac{C_D}{(C_L/n)} \right) \cdot d \tag{34}$$

Similarly, if the consumed energy (W) equals to the extracted energy (E), combined with Eqs. (12), (34),

$$d = \frac{\int_0^T \beta V^2 \sin \gamma \cos \gamma \cos \psi dt}{g \cdot \left( \frac{C_D}{(C_L/n)} \right)} \tag{35}$$

From Eq. (35), it can be found that the flight distance is a multi parameters optimization problem. The paper seeks to maximum the distance of a dynamic soaring cycle. The problem is studied through,

$$\max J = d_f \tag{36}$$

subject to Eqs. (9).  $d_f$  is the maximum distance. The constraint conditions are listed in Part 2.3. The aircraft returns to its original kinematic velocity state and height, but not the original position.

### ***2.5 Nonlinear optimal control problems of dynamic soaring***

Dynamic soaring represents a difficult control problem due to the aerobatic nature of the manoeuver and nonlinearity of the aerodynamics. In this paper, the optimal control is converted into a parameter optimization problem and solve it using an existing nonlinear programming code. Firstly, the time interval of the optimal problem is divided into a number of prescribed subintervals, the times at the ends of the subintervals are called nodes. Secondly, the control parameters and state

parameters at the nodes are chosen to form the control and state histories by interpolation. Thirdly, the state equations of the optimal problem are integrated, and the nonlinear programming code iterates on the unknown programming code iterates on the unknown parameters until the parameter optimization problem is solved [Hull (1997)].

The conversion of an optimal control problem into parameter optimization using the collocation approach begins with the definition of a series of N time points within the solution time interval [0, tf].

Values of state and control variables at each time point become solution parameters:

$$u = \begin{bmatrix} x_0 & \cdots & x_i & \cdots & x_N \\ y_0 & \cdots & y_i & \cdots & y_N \\ z_0 & \cdots & z_i & \cdots & z_N \\ V_0 & \cdots & V_i & \cdots & V_N \\ \psi_0 & \cdots & \psi_i & \cdots & \psi_N \\ \gamma_0 & \cdots & \gamma_i & \cdots & \gamma_N \\ C_{L0} & \cdots & C_{Li} & \cdots & C_{LN} \\ \phi_0 & \cdots & \phi_i & \cdots & \phi_N \end{bmatrix} \tag{37}$$

u has 8(N+1) variables. Putting all of the unknown parameters together, there is,

$$X = \begin{bmatrix} x_0 & \cdots & x_i & \cdots & x_N \\ y_0 & \cdots & y_i & \cdots & y_N \\ z_0 & \cdots & z_i & \cdots & z_N \\ V_0 & \cdots & V_i & \cdots & V_N \\ \psi_0 & \cdots & \psi_i & \cdots & \psi_N \\ \gamma_0 & \cdots & \gamma_i & \cdots & \gamma_N \\ C_{L0} & \cdots & C_{Li} & \cdots & C_{LN} \\ \phi_0 & \cdots & \phi_i & \cdots & \phi_N \\ t_0 & \cdots & t_i & \cdots & t_N \end{bmatrix} \tag{38}$$

which has 9(N+1) variables. The normalized equations of motion (Eqs. (9)) can be expressed as

$$U = f(u) \tag{39}$$

Implicit integration of Eq. (39) is performed by calculating the residuals and driving them to zero as a part of the optimization process. For the second-order mid-point rule, which has one of function evaluation at tm, the integration formula is applied in the form

$$K_m = X_{k+1} - X_k - f_m(t_{k+1} - t_k) \tag{40}$$

where

$$f_m = f(u_m) \tag{41}$$

and

$$t_m = \frac{t_k + t_{k+1}}{2}, \quad u_m = \frac{u_k + u_{k+1}}{2} \tag{42}$$

The residual is given by

$$K_m = X_{k+1} - X_k - \frac{1}{2} (f_k + f_{k+1}) (t_{k+1} - t_k) \tag{43}$$

According to the fourth-order Simpson one-third rule, the residual is

$$K_m = X_{k+1} - X_k - \frac{1}{6} (f_k + f_m + f_{k+1}) (t_{k+1} - t_k) \tag{44}$$

$f_m$  is evaluated at

$$\begin{cases} t_m = \frac{t_k + t_{k+1}}{2} \\ X_m = \frac{X_k + X_{k+1}}{2} - \frac{1}{8} (f_{k+1} - f_k) (t_{k+1} - t_k) \\ u_m = \frac{u_k + u_{k+1}}{2} \end{cases} \tag{45}$$

The path constraints in Equations (9) are enforced at the series of discrete time points as bounds on the solution parameters. In the development of a numerical integrator, it is assumed that  $u(t)$  is known so that the way in which  $u_m$  is computed does not affect the order of the integrator. For the midpoint rule, the  $u_m$  would be the parameters instead of the  $u_k$ . The converted parameter optimization problem may then be stated in the Eqs. (31) and (36).

### 3 Characteristics of optimal control problem

Because dynamic soaring flight is directly inspired by albatross, wandering albatross' parameters used by Sachs [Sachs (2005)] are assumed. Based on the architecture of a wandering albatross, a soaring aircraft model is used. The soaring aircraft model has similarities in dimension as well as the performances with albatross. This will ensure that the performances of the model are achievable by an engineering-designed aircraft. The parameter values of soaring aircraft model are repeated in Table 1.

This is a small UAV, which is designed by referring to the shape of a Wandering Albatross. According to the parameters of UAV, the dynamic soaring model is emulated by means of MATLAB. The toolbox used for the simulation is GPOPS

Table 1: The soaring aircraft model parameter values used.

Parameter	Value
Mass [kg]	8.5
Wing Area $S$ [m <sup>2</sup> ]	0.65
Aspect Ratio	16.81
Span [m]	3.306
$\rho$ [kg/m <sup>3</sup> ]	1.22
$C_{D0}$	0.033
$E_{max}$	20

(General Pseudospectral Optimal control Software) [Patterson and Rao (2013)]. The GPOPS library uses SNOPT to perform the optimization.

The basic characteristics of engineless dynamic soaring flights of UAVs through wind gradients mainly include: trajectory, airspeed, the change of attitude angles and so on.

First of all, under the restrictions of the model and boundary conditions, three three-dimensional trajectories are acquired, as shown in Figs 24. The direction of  $X$  is the the direction of wind. Fig. 2 is the trajectory of long endurance, which can be called as open long endurance trajectory.

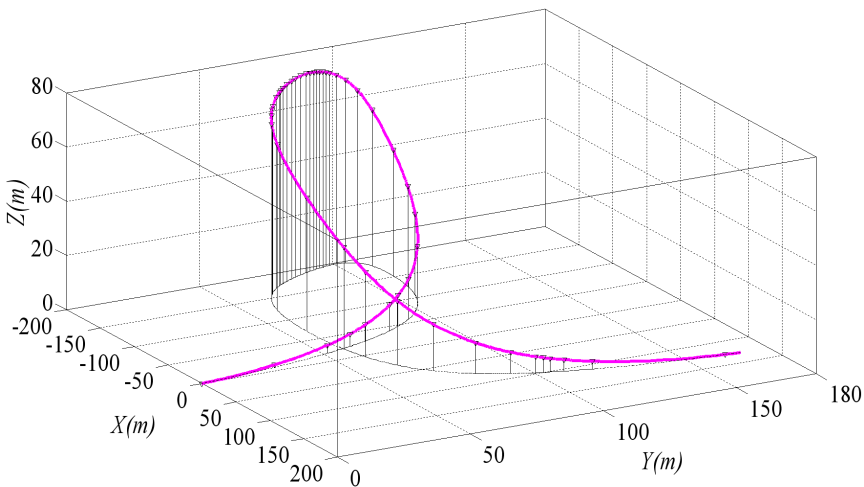


Figure 2: The trajectory for pattern (i).

After a cycle of flight, the aircraft doesn't return to the initial position. The flight distance in Fig. 2 is about 210 m.

The trajectory in Fig. 3 can be called as closed long endurance trajectory.

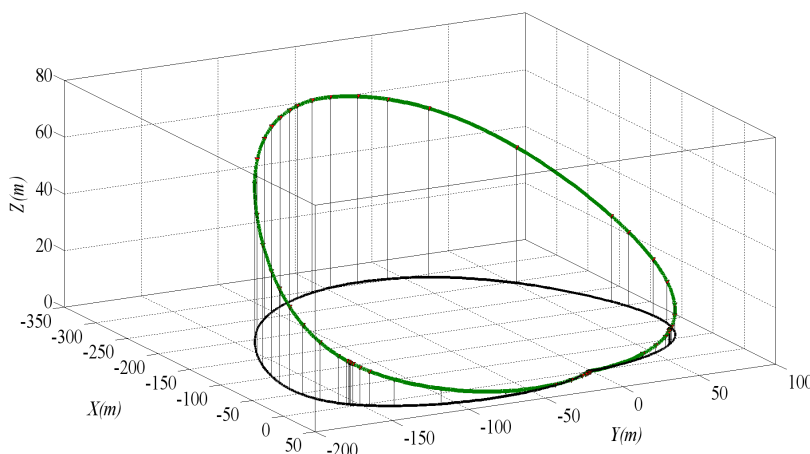


Figure 3: The trajectory for pattern (ii).

The optimization goal in Fig. 3 is the same as Fig. 2. Due to the different terminal constraints, the UAV returns to original position after a cycle of flight. This pattern of dynamic soaring is suitable for long time cruising in somewhere.

Under restriction of Eq. (36), the trajectory for maximum distance is acquired, as shown in the Fig. 4, which can be called as long distance trajectory.

Compared with Fig. 3, the aircraft did not come back to the initial position after a cycle of flight. The flight distance of Fig. 4 is over 260 m, which is farther than Fig. 2. This pattern of dynamic soaring is suitable for long distance flight.

In the simulation, the initial airspeed of the aircraft is 46.9 m/s, the aircraft's airspeed variations in three dynamic soaring cycles are shown in Fig. 5.

In Fig. 5,  $V_1$  and  $V_2$  are the airspeed for long endurance pattern of dynamic soaring in a log cycle,  $V_1$  corresponds to pattern (i),  $V_2$  corresponds to pattern (ii). Naturally,  $V_3$  is the airspeed for pattern (iii). After one cycle of flight, the aircraft's airspeed of three patterns are the same as the initial speed. That to say, even there is no motivation offered, the aircraft can achieve the goals of long distance and long endurance by means of dynamic soaring, although there have drag to consume energy. In addition, from Fig. 5, it can be found that the cycle length of pattern (iii) is shorter than other patterns. That is to say, long endurance and long distance are two independent flight patterns.

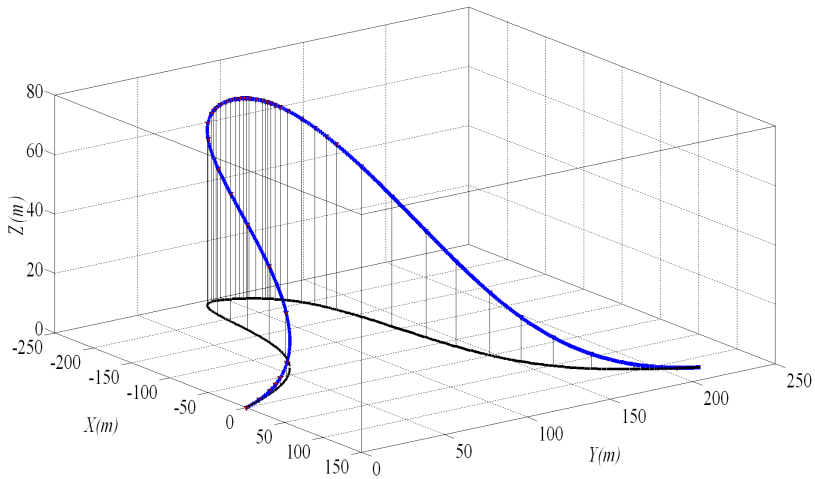


Figure 4: The trajectory for pattern (iii).

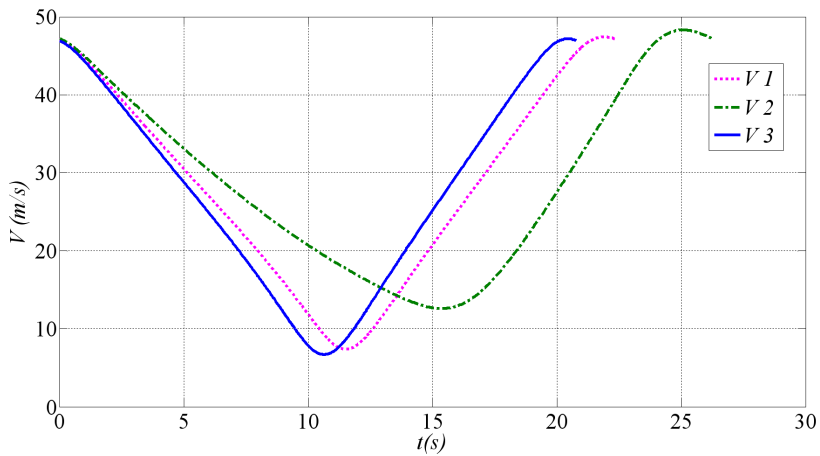


Figure 5: Airspeeds for the aircraft flying through three log cycles.

In three dynamic soaring cycles, the aircraft’s flight path angle ( $\gamma$ ), bank angle ( $\phi$ ) and heading angle ( $\psi$ ) are shown in Figs. 6-8. In Figs. 6-10, (i) represents pattern (i), (ii) represents pattern (ii), and (iii) represents pattern (iii).

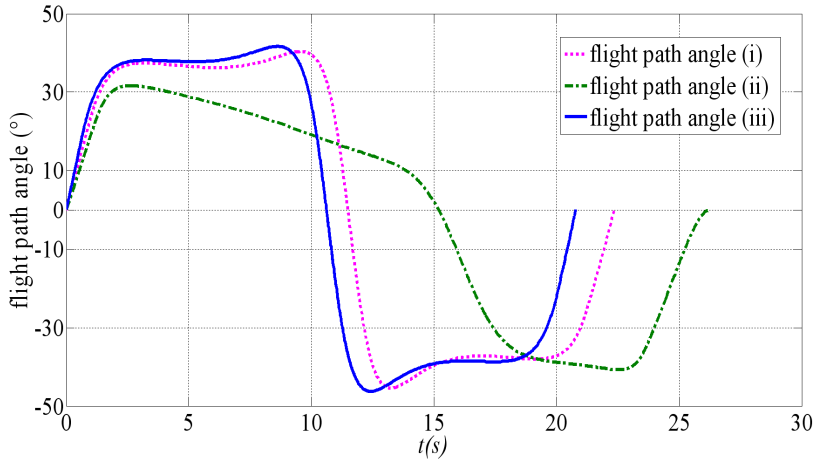


Figure 6: The flight path angle of dynamic soaring.

In Fig. 6, the variations of the flight path angles for three trajectories are almost the same. For comparison the trend of open trajectory is steeper than closed trajectory. Associated with Figs. 2-4, the closed long endurance trajectory is more smoothly.

The bank angle, which is also called as roll angle. When turning, an additional sideways motion is imparted on the aircraft. To complete the turning, the aircraft must be banked to an angle at which the total lift supports both the weight of the aircraft and the pull of the turn. From Fig. 7, it can be found that the closed long endurance trajectory is roughly circular in stimulation. In contrast, there exist fast turns in the process of open long endurance trajectory and long distance trajectory.

Fig. 8 is the historical time of heading angle of dynamic soaring, providing more attitude angle information of the motion. The heading angle variation of long endurance dynamic soaring is not a periodic process, which is a wide range process compared with long distance dynamic soaring.

The variations of lift coefficient in the process of dynamic soaring is shown in Fig. 9.

The optimal behaviour of the controls is illustrated in Fig. 4 and Fig. 9. Especially in Fig. 9, in the upper curve of the dynamic soaring, the maximum lift coefficient is reached, including long endurance and long distance. During the upper curve, the aircraft’s airspeed reaches the minimum value, in order to make sure the aircraft

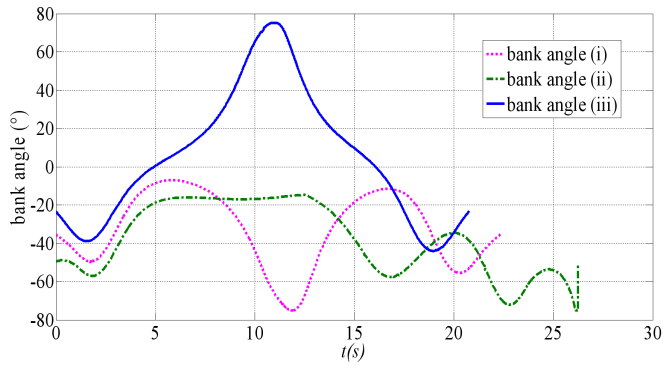


Figure 7: The bank angle of dynamic soaring.

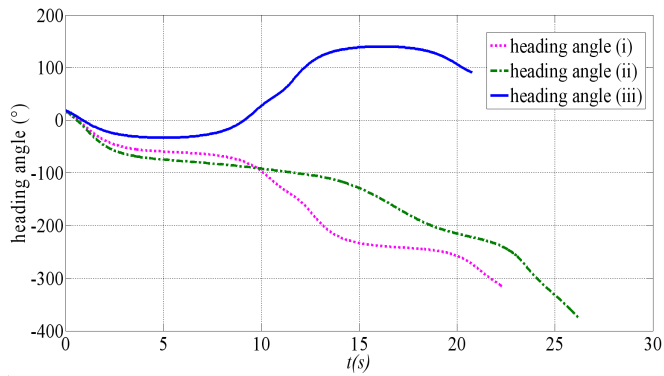


Figure 8: The heading angle of dynamic soaring.

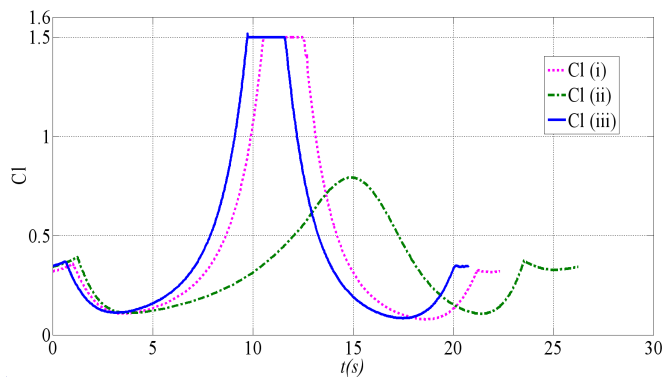


Figure 9: The lift coefficients for the aircraft flying through three log cycles.

still has enough lift for flight, it need to increase the lift coefficient. Of course, the maximum value of the lift coefficient cannot be more than boundary value (1.5). In Fig. 9, the maximum value of lift coefficient for closed long endurance trajectory is less than other two, because the minimum value of airspeed for closed long endurance trajectory is bigger than long diatance. That means the course of closed long endurance trajectory is smoother than open long endurance trajectory and long diatance trajectory.

The historical time of the load factor during three optimal dynamic soaring cycles is shown in Fig. 10.

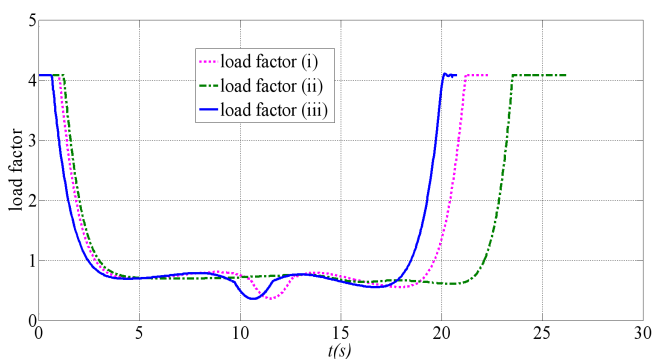


Figure 10: Load factor for the aircraft flying through three log cycles.

The variations of load factor for the long endurance is basically the same as the long distance. Load factor is not only a structural design parameter of the aircraft, but also implied by the bank angle. Compared with Fig. 7, it can be found that when the bank angle appears rapid changes, in Fig. 10, the load factor also has rapid changes. Such as at the time of 11s and 12s. The maximum value of load factor cannot be exceed 5. The values of load factor remain at 0.9 in the most of the cycle time.

Over three dynamic soaring cycles, the energy dissipated by the drag is illustrated in Fig. 11. Energy rate 1 corresponds to pattern (i), energy rate 2 corresponds to pattern (ii), energy rate 3 corresponds to pattern (iii).

From Fig. 11, it can be found that the energy variations for three patterns of dynamic soaring are similar. In the top of the flight trajectory, the energy loss due to drag in open trajectory is greater than closed trajectory. At the time of 11s and 16s, in the two patterns of long endurance of dynamic soaring, the energy loss rate due to drag close to zero, that is to say, there is no drag in this moment. The long endurance of dynamic soaring is an effective energy saving flight.

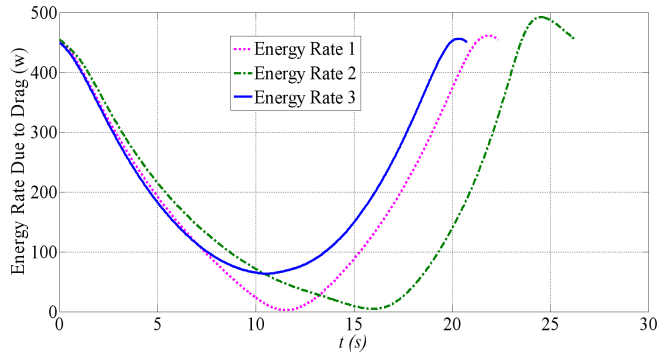


Figure 11: Energy variations due to drag in three dynamic soaring cycles.

Table 2: The comparisons of three patterns.

Parameters	Pattern (i)	Pattern (ii)	Pattern (iii)
Initial airspeed	46.9 (m/s)	46.9 (m/s)	46.9 (m/s)
Destination airspeed	46.9 (m/s)	46.9 (m/s)	46.9 (m/s)
Initial height	0 (m)	0 (m)	0 (m)
Destination height	0 (m)	0 (m)	0 (m)
The minimum airspeed	11.6 (m/s)	7.2 (m/s)	6.7 (m/s)
The maximum lift coefficient	1.5	0.8	1.5
The maximum attitude	63 (m)	59 (m)	65 (m)
The cycle length	23.5 (s)	26.5 (s)	21 (s)
The flight distance	210 (m)	0 (m)	261 (m)
The energy loss	0 (J)	0 (J)	0 (J)

Table 2 summarizes the characteristic parameters comparisons between three patterns.

From Table 2, it can be found that there is no energy loss in three patterns of dynamic soaring, which are suitable for unpowered flight. In comparison, although the cycle of long distance is shorter than long endurance, the aircraft can keep going for a long distance in a short cycle time.

#### 4 Conclusions

Dynamic soaring gives the engineless UAV an ability to extract energy from the environment, thus prolonging its endurance and distance. In the dynamic model of engineless UAV in gradient wind field, a fictitious force produced by wind gradient

is positive work force. The energy extracted from the wind field depends on the product of heading angle and flight path angle. Long endurance and long distance trajectory optimization in dynamic soaring are formulated as non-linear optimal control problems, which include two optimization formulas and two kinds of terminal constraints. The method of collocation approach is used to convert these problems into parameters optimization for numerical solutions.

Three optimal patterns of dynamic soaring are presented. Three energy-gaining trajectories are ones in which the UAV passes through gradients with specific conditions on its relative orientation (heading angle, flight path angle and bank angle), aerodynamic load factor, and airspeed and so on. In patterns (i) and (ii), the endurance equations for aircraft are optimized as nonlinear problems. When the aircraft doesn't return to the original position, patterns (i) occurs. Pattern (ii) results when the aircraft returns to original position. Patterns (iii) occurs when the distance equations are optimized. In three patterns, the aircraft gains the maximum flight time in pattern (ii), in pattern (iii), the aircraft gains the maximum flight distance. According to the energy variations for three patterns, the closed trajectory for long endurance is an effective energy saving flight.

Three optimal patterns of dynamic soaring are presented. Three energy-gaining trajectories are ones in which the UAV passes through gradients with specific conditions on its relative orientation (heading angle, flight path angle and bank angle), aerodynamic load factor, and airspeed and so on. In patterns (i) and (ii), the endurance equations for aircraft are optimized as nonlinear problems. When the aircraft doesn't return to the original position, patterns (i) occurs. Pattern (ii) results when the aircraft returns to original position. Patterns (iii) occurs when the distance equations are optimized. In three patterns, the aircraft gains the maximum flight time in pattern (ii), in pattern (iii), the aircraft gains the maximum flight distance. According to the energy variations for three patterns, the closed trajectory for long endurance is an effective energy saving flight.

Finally, in order to make dynamic soaring profit from further research work as soon as possible, some future work should be done, such as the accurate model of wind field, more dynamic soaring experiments and so on.

## References

**Akhtar, N.; James, W.; Alastair, C.** (2009): Wind Shear Energy Extraction using Dynamic Soaring Techniques. AIAA Aerospace Sciences Meeting including The New Horizons Forum and Aerospace Exposition, pp. 1-15.

**Bencatel, R.; Kabamba, P.; Girard, A.** (2014): Perpetual Dynamic Soaring in Linear Wind Shear. *Journal of Guidance, Control, and Dynamics*, vol. 37, no. 5,

pp. 1712-1716.

**Bower, G. C.** (2011): Boundary Layer Dynamic Soaring for Autonomous Aircraft: Design and Validation. PhD thesis, Stanford University, Stanford.

**Clarence, J. D. C.** (1964): A Mathematical Analysis of the Dynamic Soaring Flight of the Albatross with Ecological Interpretations. Virginia Institute of Marine Science.

**Deittert, M.; Richards, A.; Toomer, C. A.** (2009): Engineless Unmanned Aerial Vehicle Propulsion by Dynamic Soaring. *Journal of Guidance, Control and Dynamics*, vol. 32, no. 5, pp. 1446-1457.

**Denny, M.** (2009): Dynamic soaring: aerodynamics for albatrosses. *European Journal of Physics*, vol. 30, pp. 75-84.

**Guo, W.; Zhao, Y. J.** (2010): Optimal Unmanned Aerial Vehicle Flights for Seability and Endurance in Winds. *Journal of Aircraft*, vol. 48, pp. 305-314.

**Hull, D. G.** (1997): Conversion of Optimal Control Problems into Parameter Optimization Problems. *Journal of Guidance, Control, and Dynamics*, vol. 20, pp. 57-60.

**José, J. V.; Saletan, E. J.** (1998): *Classical Dynamics: A Contemporary Approach*. Cambridge University Press, pp. 39-40.

**Kermode, A. C.** (2006): *Mechanics of Flight*. Pitman Books Ltd, pp. 85-105.

**Lawrance, N. R. J.; Sukkarieh, S.** (2011): Path Planning for Autonomous Soaring Flight in Dynamic Wind Fields. 2011 IEEE International Conference on Robotics and Automation, pp. 2499-2505.

**Lawrance, N. R. J.; Sukkarieh, S.** (2011): Autonomous Exploration of a Wind Field with a Gliding Aircraft. *Journal of Guidance, Control and Dynamics*, vol. 34, pp. 719-723.

**Patterson, M. A.; Rao, A. V.** (2013): GPOPS - II Version 1.0: A General-Purpose MATLAB Toolbox for Solving Optimal Control Problems Using the Radau Pseudospectral Method. University of Florida, Gainesville.

**Richardson, P. L.** (2011): How do albatrosses fly around the world without flapping their wings? *Progress in Oceanography*, vol. 88, pp. 46-58.

**Rayleigh, J. W. S.** (1883): The soaring of Birds. *Nature*, vol. 27, pp. 534-535.

**Sachs, G.; Lesch, K.; Knoll, A.** (1989): Optimal Control for Maximum Energy Extraction from Wind Shear. AIAA Guidance, Navigation and Control Conference, pp. 556-561.

**Sachs, G.** (2005): Minimum shear wind strength required for dynamic soaring of albatrosses. *Ibis*, vol. 2005, pp. 1-10.

**Sachs, G.; Orlando, C.** (2003): Optimization of Dynamic Soaring at Ridges. *AIAA Atmospheric Flight Mechanics Conference and Exhibit*, pp. 1-10.

**Traugott, J.; Holzappel, F.; Sachs, G.** (2010): Conceptual Approach for Precise Relative Positioning with Miniaturized GPS Loggers and Experimental Results. RTO-EN-SET-116, pp. 4-24.

**Vincent, B.; Christine, T.; Moschetta, J. M.; Emmanuel, B.** (2013): Energy Harvesting Mechanisms for UAV Flight by Dynamic Soaring. *AIAA Atmospheric Flight Mechanics (AFM) Conference*, pp. 1-10.

**Zhao, Y. J.** (2004): Optimal patterns of glider dynamic soaring. *Optimal Control Applications and Methods*, vol.25, pp. 67-89.

**Zhao, Y. J.; Qi, Y. C.** (2004): Minimum fuel powered dynamic soaring of unmanned aerial vehicles utilizing wind gradients. *Optimal Control Application and Methods*, vol. 25, no. 5, pp. 211-233.

